

Learning interacting fermionic Hamiltonians at the Heisenberg limit

Arjun Mirani^{1,2} and Patrick Hayden^{1,3}

¹Stanford Institute for Theoretical Physics, Stanford University, Stanford, CA, USA

²Department of Applied Physics, Stanford University, Stanford, CA, USA

³Department of Physics, Stanford University, Stanford, CA, USA

March 14, 2024

Abstract

Efficiently learning an unknown Hamiltonian given access to its dynamics is a problem of interest for quantum metrology, many-body physics and machine learning. A fundamental question is whether learning can be performed at the Heisenberg limit, where the Hamiltonian evolution time scales inversely with the error, ε , in the reconstructed parameters. The Heisenberg limit has previously been shown to be achievable for certain classes of qubit and bosonic Hamiltonians. Most recently, a Heisenberg-limited learning algorithm was proposed for a simplified class of fermionic Hubbard Hamiltonians restricted to real hopping amplitudes and zero chemical potential at all sites, along with on-site interactions. In this work, we provide an algorithm to learn a more general class of fermionic Hubbard Hamiltonians at the Heisenberg limit, allowing complex hopping amplitudes and nonzero chemical potentials in addition to the on-site interactions, thereby including several models of physical interest. The required evolution time across all experiments in our protocol is $\mathcal{O}(1/\varepsilon)$ and the number of experiments required to learn all the Hamiltonian parameters is $\mathcal{O}(\text{polylog}(1/\varepsilon))$, independent of system size as long as each fermionic mode interacts with $\mathcal{O}(1)$ other modes. Unlike prior algorithms for bosonic and fermionic Hamiltonians, to obey fermionic parity superselection constraints in our more general setting, our protocol utilizes $\mathcal{O}(N)$ ancillary fermionic modes, where N is the system size. Each experiment involves preparing fermionic Gaussian states, interleaving time evolution with fermionic linear optics unitaries, and performing local occupation number measurements on the fermionic modes. The protocol is robust to a constant amount of state preparation and measurement error.

1 Introduction

The problem of learning an unknown Hamiltonian, given access to its dynamics with time-evolution as a black-box operator, is of interest to a range of fields including quantum metrology [1–14], many-body physics [15–37] and machine learning [28–34]. The Hamiltonian

learning problem can be considered a special case of quantum process tomography [38], asking whether a black-box physical process can be characterized up to some desired precision. Hamiltonian learning is increasingly of practical interest due to synthetic quantum systems and devices that need to be benchmarked [18, 39–42].

Investigating the *efficiency* of Hamiltonian learning protocols is of both fundamental and practical interest. For instance, how much total time evolution t , or how many copies n of an entangled probe quantum state, are required to learn the parameters of the Hamiltonian to error ε ? The fundamental quantum limit, representing the most efficient scaling, is the so-called ‘Heisenberg limit’, which is either $t \sim \mathcal{O}(1/\varepsilon)$ or $n \sim \mathcal{O}(1/\varepsilon)$, depending on whether time or entanglement is the metrological resource [43–45]. In the context of many-body Hamiltonians, most prior work (such as [18–29]) achieves the so-called ‘standard quantum limit’, where the total evolution time scales as $\Omega(1/\varepsilon^2)$. Only in the past two years has it been shown that the Heisenberg limit is achievable for certain classes of many-body Hamiltonians governing systems of qubits [35, 37] and bosons [36]. Notably, [37] showed that for a large set of many-body Hamiltonians, including those that thermalize via the eigenstate thermalization hypothesis, achieving the Heisenberg limit requires *quantum control*, which can be of two types, discrete or continuous. Discrete quantum control refers to interleaving time evolution with unitary gates. Continuous quantum control refers to continuously time-evolving the system under a modified Hamiltonian, where known terms are added to the original unknown Hamiltonian. The Heisenberg-limited algorithm of [35] for the qubit case and [36] for the bosonic case both involve discrete control. In these algorithms, interleaving time-evolution with suitable unitaries effectively decouples the many-body Hamiltonian into multiple non-interacting clusters, which can be learned in parallel via a divide-and-conquer approach. The Heisenberg-limited qubit algorithm of [37], on the other hand, uses continuous quantum control, allowing estimates of the Hamiltonian parameters to be adaptively refined through an iterative process.

Recently, [46] proposed a Heisenberg-limited learning algorithm for a simplified subset of *fermionic* Hubbard Hamiltonians restricted to real hopping amplitudes and zero chemical potential at all sites, along with on-site interactions.¹ In this work, we provide an algorithm to learn a more general class of fermionic Hubbard Hamiltonians at the Heisenberg limit, allowing complex hopping amplitudes and nonzero chemical potentials in addition to the on-site interactions, thereby including several systems of physical interest. The approach of [46] is similar to ours, since both works adapt the technique of discrete quantum control used in the qubit [35] and bosonic [36] settings. However, generalizing to the complex hopping amplitudes and nonzero chemical potentials of our model requires additional ingredients to obey fermionic parity superselection constraints and learn the complex coefficients. These generalizations are physically relevant – for instance, complex amplitudes are used to incorporate the effects of magnetic fields [47, 48], and nontrivial chemical potential plays a key role in the properties of metals [49]. In the disordered setting, the variation of local energy across different sites, captured by the chemical potential coefficients, contributes to phenomena such as an Anderson localization; the special case of our model in which hopping terms and local energies are assigned randomly is known as the Anderson-Hubbard

¹Our research was performed independently. We only became aware of [46] in the final stages of preparing this manuscript.

model [50, 51]. Our protocol thus extends the regime of achievability of Heisenberg-limited learning to a physically well-motivated class of fermionic Hamiltonians. Such learning algorithms could potentially play a practical role in characterizing fermionic systems in the lab and benchmarking fermionic analog quantum simulators, which offer exciting possibilities to investigate condensed matter phenomena in regimes where classical computation is challenging [52–59].

Our protocol consists of a series of experiments, each of which involves parallel preparation of two-mode fermionic Gaussian states that couple modes of the system to fermionic ancilla modes. This is followed by interleaving time evolution with fermionic linear optics (FLO) unitaries, and performing local occupation number measurements on the fermionic modes. The measurement results are efficiently post-processed classically according to the Heisenberg-limited Robust Phase Estimation (RPE) algorithm [43–45]. Overall, the protocol utilizes $\mathcal{O}(N)$ ancillae, where N is the system size, although many of the experiments require no ancillae at all. The total time evolution across all experiments scales as $\mathcal{O}(1/\varepsilon)$ and the number of experiments scales as $\mathcal{O}(\text{polylog}(1/\varepsilon))$. As long as the degree of the graph of interactions is bounded, these complexities are independent of the system size. Furthermore, our protocol is robust to a constant amount of state preparation and measurement error, a feature inherited from the robustness of RPE.

The rest of this paper is structured as follows: Section 2.1 specifies the class of fermionic Hamiltonians under consideration and provides a statement of results. Sections 2.2 to 2.4 describe the learning algorithm in a step-by-step manner, each section describing a subroutine that is used by the next, culminating in a divide-and-conquer approach to learning the full many-body Hamiltonian. Section 3 concludes with a summary and discussion of future directions. Finally, Appendices 3 and 3 discuss the boundedness of the errors in the reconstructed parameters of the Hamiltonian.

2 Results

2.1 Model and statement of results

The interacting fermionic Hamiltonians considered in this paper are of the following form, representing the Hubbard model:

$$H = \sum_{\langle i,j \rangle} \sum_{\sigma \in \{\uparrow, \downarrow\}} h_{ij\sigma} a_{i\sigma}^\dagger a_{j\sigma} + \sum_{\sigma \in \{\uparrow, \downarrow\}} \omega_{i\sigma} n_{i\sigma} + \sum_i \xi_i n_{i\uparrow} n_{i\downarrow} \quad (1)$$

The indices i, j denote spatial sites, corresponding to the vertices of a bounded-degree graph. Each spatial site comprises two spin modes with opposite spins (\uparrow and \downarrow). The pair $\langle i, j \rangle$ denotes vertices connected by an edge in the underlying graph, generalizing the nearest-neighbor relation on a lattice. The operators $a_{i\sigma}^\dagger$ and $a_{i\sigma}$ are respectively the creation and annihilation operators for the fermionic spin mode at site i with spin σ . They satisfy the canonical anticommutation relations: $\{a_{i\sigma}, a_{j\rho}^\dagger\} = \delta_{ij} \delta_{\sigma\rho}$, while all other anticommutators vanish. The operator $n_{i\sigma} = a_{i\sigma}^\dagger a_{i\sigma}$ is the number operator for the corresponding spin mode. Due to the hermiticity of the Hamiltonian, the coefficients $h_{ij\sigma}^* = h_{ji\sigma}$ while $\omega_{i\sigma}$ and ξ_i are real. We use similar notation to [36] for the coefficients to highlight the analogy to the bosonic

case. In physical terms, the $h_{ij\sigma}$ coefficients are hopping amplitudes, the $\omega_{i\sigma}$ coefficients are chemical potentials, and the ξ_i coefficients represent on-site interaction strength [60].

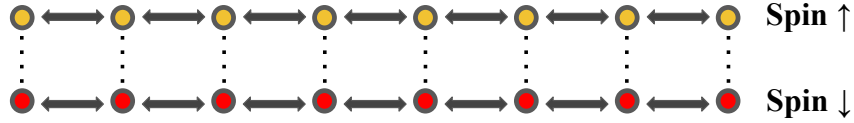


Figure 1: Diagrammatic representation of a fermionic Hubbard Hamiltonian defined on a one-dimensional lattice. The yellow and red modes correspond to opposite spins. Dotted lines represent on-site repulsion between modes of opposite spin with the same spatial index. Arrows represent hopping interactions between neighboring spatial sites. For Hamiltonians defined on a more general graph, any two sites linked by an edge have a hopping interaction.

Given access to black box time evolution generated by a Hamiltonian of the form in Eq. (1), our goal is to learn the parameters $h_{ij\sigma}$, $\omega_{i\sigma}$ and ξ_i for all the fermionic modes, with root-mean-square error upper bounded by some ε . In Sections 2.2 to 2.4 below, we describe a protocol that achieves this, assuming the ability to:

1. prepare two-mode fermionic Gaussian states of the system and ancilla modes;
2. apply black box time evolution under the unknown Hamiltonian;
3. apply specified two-mode unitaries of the fermionic linear optics (FLO) form;
4. perform local occupation measurements on the system and ancilla modes.

The total amount of evolution time scales as $\mathcal{O}(1/\varepsilon)$, the Heisenberg limit. The number of experiments required is $\mathcal{O}(\text{polylog}(1/\varepsilon))$. Some of the experiments utilize $\mathcal{O}(N)$ ancillae, which can be re-used across multiple experiments. Additionally, the protocol is robust to a constant amount of state preparation and measurement (SPAM) error.

We will begin by discussing the simplest example of our class of Hamiltonians in Section 2.2 – namely, a fermionic quantum anharmonic oscillator Hamiltonian with a single spatial site. Next, we will consider a two-site coupled anharmonic oscillator Hamiltonian in Section 2.3, and show how this can be reduced to the single-site case. Using these results, in Section 2.4 we show how the many-body Hamiltonians described by Eq. (1) can be reduced to the two-site case, facilitating parallelized learning of the Hamiltonian coefficients. Appendices 3 and 3 discuss the boundedness of the errors in the reconstructed parameters of the Hamiltonian.

2.2 Learning a single-site (two-mode) Hamiltonian

We begin by considering a single-site anharmonic oscillator Hamiltonian. The protocol to learn its parameters will be a core subroutine for the many-body case. Labelling the two spin modes of the single site as 1 and 2, as shown in Fig. 2, the single-site Hamiltonian is

$$H = \omega_1 n_1 + \omega_2 n_2 + \xi_{12} n_1 n_2. \quad (2)$$

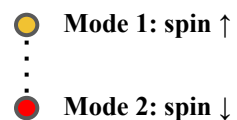


Figure 2: Diagrammatic representation of the single-site Hamiltonian in Eq. (2).

Note the slight change in notation relative to Eq. (1): for simplicity, the subscripts 1 and 2 denote spin modes at the same spatial site, and there is no explicit spatial index. The only interaction term in this Hamiltonian is the on-site interaction $\xi_{12}n_1n_2$ between spin modes 1 and 2.

The parameters of this Hamiltonian can be learned using the robust phase estimation (RPE) algorithm of [43] (further analyzed and developed by [44, 45, 61]). RPE enables us to achieve Heisenberg scaling, and we provide a very brief review of the key ideas here. The goal is to estimate an unknown phase $\omega \in [-1, 1]$, given the ability to apply a unitary of the form $U_\omega = e^{-i\omega H}$ (where H is Hermitian) to a probe state $|\psi_0\rangle$ of our choosing and perform measurements on the resulting state. Depending on whether the metrological resource available is time or entanglement, either U_ω is applied multiple times to a single probe state (which can be viewed as applying the time evolution operator $e^{-i\omega Ht}$ for some time t), or many copies of U_ω are simultaneously applied to multiple copies of multiple entangled probes. In this work we restrict our attention to the former case, where time is the resource. The RPE protocol requires performing multiple rounds of such experiments, with the rounds grouped into generations characterized by different amounts of evolution time. Suppose there are M generations of experiments, where generation j involves m_j experiments, each of which involves time evolution $e^{-i\omega Ht_j}$ for time t_j . The total time used for time evolution is $t_{\text{tot}} = \sum_1^M m_j t_j$. By the end of the process, we have an estimator $\tilde{\omega}$ of the true phase ω , with some standard deviation $\Delta\tilde{\omega}$. The key point is that, as discussed in [43, 45], the parameters m_j and t_j can be chosen such that $\Delta\tilde{\omega} \leq \mathcal{O}(1/t_{\text{tot}})$, which is the statement that RPE achieves Heisenberg scaling. More details on how to choose the specific values of these parameters can be found in [43–45, 61].

In the approach to RPE of [43–45], the measurement step in each experiment above is designed to output a Bernoulli random variable with a particular probability distribution. In particular, in each generation of experiments, one performs two types of experiments: “Type-0” (with measurement outcomes labelled by 0 and 1) and “Type-+” (with measurement outcomes + or –). Their output probabilities in the j^{th} generation of experiments are given by

$$\begin{aligned} p_0(\omega, j) &= \frac{1}{2}(1 + \cos(\omega t_j)) + \delta_0(j) \\ p_+(\omega, j) &= \frac{1}{2}(1 + \sin(\omega t_j)) + \delta_+(j) \end{aligned} \tag{3}$$

where δ_0, δ_+ represents additive noise, such as state-preparation-and-measurement (SPAM) error. As long as δ_0 and δ_+ are bounded by a small constant, the measurement outcomes obeying the above distribution can be post-processed to yield an estimate of ω with Heisenberg scaling. This is done by repeatedly halving the size of the confidence interval for ω using the outcomes of each successive generation of experiments. For a more detailed review of RPE we refer the reader to [43–45, 61].

Returning to our problem of learning the parameters ω_1, ω_2 , and ξ_{12} of the Hamiltonian in Eq. (2), we use RPE to learn them one by one. In each case, we must design an experiment involving an appropriate initial state of the fermionic system, and choice of measurements, such that we obtain the desired Type-0 and Type-+ measurement statistics. We do this by preparing an initial state which, under time evolution, picks up a relative phase that depends in a known way on the Hamiltonian parameter to be learned, and measure the time-evolved

state in bases that yield the desired statistics.

Starting with ω_1 , we assume the availability of a fermionic ancilla spin mode, to which can couple a spin mode of our system. Let b^\dagger and b respectively denote the creation and annihilation operators for the ancilla mode. To express our initial state and measurement basis, we define the following two-mode unitaries, which act on system mode 1 and the ancilla mode:

$$\begin{aligned} V(\theta) &= e^{\theta(a_1^\dagger b^\dagger - b a_1)} \\ W(\theta) &= e^{i\theta(a_1^\dagger b^\dagger + b a_1)} \end{aligned} \quad (4)$$

For $\theta = -\frac{\pi}{4}$, V and W apply the following transformations to $|\Omega\rangle$, the vacuum state of the entire system (original system plus ancilla):

$$\begin{aligned} V(-\frac{\pi}{4})|\Omega\rangle &= \frac{1}{\sqrt{2}}(|\Omega\rangle + a_1^\dagger b^\dagger |\Omega\rangle) \\ W(-\frac{\pi}{4})|\Omega\rangle &= \frac{1}{\sqrt{2}}(|\Omega\rangle - i a_1^\dagger b^\dagger |\Omega\rangle) \end{aligned} \quad (5)$$

These are equally weighted superpositions of the vacuum state and the state with both modes occupied. They belong to the well-known class of fermionic Gaussian states [62].

Now, choose the initial state to be $V(-\frac{\pi}{4})|\Omega\rangle$. Next, induce dependence on the parameter ω_1 by applying the time evolution operator e^{-iHt} , where H is the Hamiltonian from Eq. (2):

$$e^{-iHt}(V(-\frac{\pi}{4})|\Omega\rangle) = \frac{1}{\sqrt{2}}(|\Omega\rangle + e^{-i\omega_1 t} a_1^\dagger b^\dagger |\Omega\rangle) \quad (6)$$

For the Type-0 measurement, apply $V^\dagger(-\frac{\pi}{4})$, then measure the occupation numbers of system mode 1 and the ancilla mode. The probability of obtaining $|\Omega\rangle$ as the final state (corresponding to no occupation) is given by

$$p_0 = |\langle\Omega| V^\dagger(-\frac{\pi}{4}) e^{-iHt} V(-\frac{\pi}{4}) |\Omega\rangle|^2 = \frac{1}{2}(1 + \cos(\omega_1 t)). \quad (7)$$

For the Type-+ measurement, apply $W^\dagger(-\frac{\pi}{4})$, then measure the occupation numbers of system mode 1 and the ancilla mode. The probability of obtaining $|\Omega\rangle$ as the final state (interpreted as the “+”-outcome due to the effective basis change implemented by W^\dagger) is

$$p_+ = |\langle\Omega| W^\dagger(-\frac{\pi}{4}) e^{-iHt} V(-\frac{\pi}{4}) |\Omega\rangle|^2 = \frac{1}{2}(1 + \sin(\omega_1 t)). \quad (8)$$

In practice, the probabilities above will be shifted by additive noise terms, as in Eq. (3), corresponding to SPAM error (which, as discussed above, do not affect the RPE protocol as long as they are bounded by a small constant). With measurement statistics of this form, we can perform robust phase estimation as described above to learn ω_1 with Heisenberg scaling.

The discussion above also clarifies the utility of the ancilla. From a purely mathematical perspective, a more natural initial state to use would be $e^{\theta(a_1 - a_1^\dagger)} |\Omega\rangle = \frac{1}{\sqrt{2}}(|\Omega\rangle + a_1^\dagger |\Omega\rangle)$. Then, replacing $V(\theta)$ by $e^{\theta(a_1 - a_1^\dagger)}$ and $W(\theta)$ by $e^{i\theta(a_1 + a_1^\dagger)}$ in the expressions above, would yield the same values for p_0 and p_+ as obtained in Eq. (7) and Eq. (8). This approach seems

simpler, as it does not require an ancilla, and the unitaries V and W act only on a single mode. However, the unitaries V and W are unphysical, because they can be used to prepare a superposition of an odd-parity and even-parity state, as we just saw. These states belong to an unphysical sector of our fermionic Hilbert space, because their existence would enable violations of the no-signalling principle [63]. This *parity superselection rule* forces us to use either odd parity or even parity states. If we prepared such states using just the system modes, the phases resulting from time evolution would involve linear combinations of the unknown coefficients. Therefore, to isolate ω_1 , we couple to the ancilla. However, this is not necessary for ω_2 , as we discuss below.

To learn the parameter ω_2 , there are two approaches: with or without the ancilla. The first option, which uses the ancilla, is to simply perform the same procedure described above, but interchanging the roles of modes 1 and 2. The second option is to use a different initial state that only involves the system (no ancilla), and takes advantage of the fact that we have already learned ω_1 . In particular, instead of using the V and W defined in Eq. (4), we define new two-mode unitaries V' and W' , which are fermionic beamsplitter operations acting on system modes 1 and 2:

$$\begin{aligned} V'(\theta) &= e^{\theta(a_1^\dagger a_2 - a_2^\dagger a_1)} \\ W'(\theta) &= e^{i\theta(a_1^\dagger a_2 + a_2^\dagger a_1)} \end{aligned} \quad (9)$$

For $\theta = -\frac{\pi}{4}$, V' and W' apply the following transformations to the initial state with only mode 1 occupied, $a_1^\dagger |\Omega\rangle$:

$$\begin{aligned} V'(-\frac{\pi}{4})(a_1^\dagger |\Omega\rangle) &= \frac{1}{\sqrt{2}}(a_1^\dagger |\Omega\rangle + a_2^\dagger |\Omega\rangle) \\ W'(-\frac{\pi}{4})(a_1^\dagger |\Omega\rangle) &= \frac{1}{\sqrt{2}}(a_1^\dagger |\Omega\rangle - ia_2^\dagger |\Omega\rangle) \end{aligned} \quad (10)$$

The initial and final states in Eq. (10) are both odd-parity states, so these states and operations satisfy the parity superselection rule. Now, the parameter-dependence induced by time evolving the state $V'(-\frac{\pi}{4})(a_1^\dagger |\Omega\rangle)$ under e^{-iHt} is

$$e^{-iHt}V'(-\frac{\pi}{4})(a_1^\dagger |\Omega\rangle) = \frac{1}{\sqrt{2}}(e^{-i\omega_1 t}a_1^\dagger |\Omega\rangle + e^{-i\omega_2 t}a_2^\dagger |\Omega\rangle) = \frac{1}{\sqrt{2}}e^{-i\omega_1 t}(a_1^\dagger |\Omega\rangle + e^{-i(\omega_2 - \omega_1)t}a_2^\dagger |\Omega\rangle). \quad (11)$$

For the Type-0 measurement, apply $V'^\dagger(-\frac{\pi}{4})$ after time evolution, then measure the occupation numbers of modes 1 and 2. The probability obtaining the state $a_1^\dagger |\Omega\rangle$ upon measurement (mode 1 occupied, mode 2 unoccupied) is given by

$$p_0 = |(\langle \Omega | a_1) V'^\dagger(-\frac{\pi}{4}) e^{-iHt} V'(-\frac{\pi}{4})(a_1^\dagger |\Omega\rangle)|^2 = \frac{1}{2}(1 + \cos((\omega_2 - \omega_1)t)). \quad (12)$$

For the Type-+ measurement, apply $W'^\dagger(-\frac{\pi}{4})$ after time evolution, then measure the occupation numbers of modes 1 and 2. The probability of obtaining $a_1^\dagger |\Omega\rangle$ upon measurement is

$$p_+ = |(\langle \Omega | a_1) W'^\dagger(-\frac{\pi}{4}) e^{-iHt} V'(-\frac{\pi}{4})(a_1^\dagger |\Omega\rangle)|^2 = \frac{1}{2}(1 + \sin((\omega_2 - \omega_1)t)). \quad (13)$$

Applying RPE to the measurement statistics, as described previously, provides an estimate of $(\omega_2 - \omega_1)$ with Heisenberg scaling. Adding this to the previously estimated value of ω_1 provides an estimate of ω_2 . Appendix 3 discusses the RMS error of such linear combinations of estimators.

Finally, to learn the last coupling coefficient ξ_{12} , no ancilla is needed. The procedure is almost the same as that for ω_1 , the only difference being that the unitaries $V(-\frac{\pi}{4})$ and $W(-\frac{\pi}{4})$ defined in Eq. (4) now act on the two system modes (that is, b in Eq. (4) is replaced by a_2). The Type-0 and Type-+ measurement probabilities are:

$$\begin{aligned} p_0 &= |\langle \Omega | V^\dagger(-\frac{\pi}{4}) e^{-iHt} V(-\frac{\pi}{4}) | \Omega \rangle|^2 = \frac{1}{2} (1 + \cos((\omega_1 + \omega_2 + \xi_{12})t)) \\ p_+ &= |\langle \Omega | W^\dagger(-\frac{\pi}{4}) e^{-iHt} V(-\frac{\pi}{4}) | \Omega \rangle|^2 = \frac{1}{2} (1 + \sin((\omega_1 + \omega_2 + \xi_{12})t)) \end{aligned} \quad (14)$$

Performing RPE with this data provides an estimate of the sum $(\omega_1 + \omega_2 + \xi_{12})$, which can be used in conjunction with the previously obtained estimates of ω_1 and ω_2 to obtain an estimate of ξ_{12} . In this way, all three unknown parameters of the single-site Hamiltonian in Eq. (2) can be learned.

2.3 Learning a two-site (four-mode) Hamiltonian

Next, consider a two-site Hamiltonian representing two coupled fermionic quantum anharmonic oscillators. Opposite-spin modes 1 and 2 constitute one spatial site, and opposite-spin modes 3 and 4 constitute the other, as shown in Fig. 3. The spin modes at a given site are coupled by an interaction term, as in Section 2.2, while modes of the same spin in adjacent sites are coupled by a hopping interaction. Thus the Hamiltonian takes the following form, where all indices refer to spin modes of the system:

$$\begin{aligned} H &= h_{13}a_1^\dagger a_3 + h_{31}a_3^\dagger a_1 + h_{24}a_2^\dagger a_4 + h_{42}a_4^\dagger a_2 \\ &+ \omega_1 n_1 + \omega_2 n_2 + \omega_3 n_3 + \omega_4 n_4 + \xi_{12} n_1 n_2 + \xi_{34} n_3 n_4 \end{aligned} \quad (15)$$

We can learn this Hamiltonian in two stages. First, we learn the coefficients of the number-conserving terms, i.e. the ω (chemical potential) and ξ (on-site interaction) coefficients in the second line of Eq. (15). This involves ‘discrete quantum control’ – reshaping the Hamiltonian using random unitaries that decouple the two spatial sites by approximately eliminating the hopping terms (as in refs [35, 36]). Next, we learn the hopping coefficients in the first line of Eq. (15), which involves performing a basis transformation and using the reshaping technique again. We elaborate on the details of this procedure below.

2.3.1 Learning coefficients of number-conserving terms

To learn the ω coefficients, we require one ancilla mode per spatial site, that is, one for system modes 1 and 2, and another for system modes 3 and 4. These ancilla modes are first

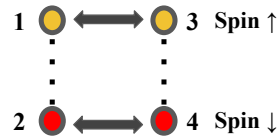


Figure 3: Diagrammatic representation of the two-site Hamiltonian in Eq. (15).

used to learn ω_1 and ω_3 in parallel. They can optionally be re-used to learn ω_2 and ω_4 in parallel, although those coefficients can be learned without ancillae as well. Finally, ξ_{12} and ξ_{34} are learned in parallel, without ancillae.

Starting with coefficients ω_1 and ω_3 , the strategy is to alternate small time-steps of Hamiltonian evolution generated by H with random unitaries sampled from a suitable distribution. The resulting time evolution is then approximately generated by a ‘reshaped’ effective Hamiltonian H_{eff} :

$$H_{\text{eff}} = \omega_1 n_1 + \omega_2 n_2 + \omega_3 n_3 + \omega_4 n_4 + \xi_{12} n_1 n_2 + \xi_{34} n_3 n_4 \quad (16)$$

Techniques to perform this reshaping, inspired by dynamical decoupling and the qDRIFT randomized compiling algorithm [64], were developed in [35] for low-intersection qubit Hamiltonians and in [36] for a class of Bose-Hubbard Hamiltonians. The latter class of Hamiltonians [36] is similar to ours. Here we show how this approach extends to the fermionic case, using fermionic analogues of the unitaries used in the bosonic case.

To perform reshaping, we begin by defining a distribution \mathcal{D} over unitaries U such that:

$$H_{\text{eff}} = \mathbb{E}_{U \sim \mathcal{D}} U^\dagger H U \quad (17)$$

where H_{eff} has the form shown in Eq. (16). In particular, the distribution that we use is defined over the following one-parameter subset of ‘fermionic linear optics’ (FLO) [62] unitaries:

$$U = e^{-i\theta(n_1+n_2)} \quad (18)$$

The distribution \mathcal{D} corresponds to $\theta \sim \mathcal{U}([0, 2\pi])$, the uniform distribution over the interval $[0, 2\pi]$. Using the following facts that hold for any fermionic mode j and any pair of distinct modes $j \neq k$:

$$\begin{aligned} e^{i\theta n_j} a_j^\dagger e^{-i\theta n_j} &= e^{i\theta} a_j^\dagger \\ [a_j, n_k] &= 0 \end{aligned} \quad (19)$$

the distribution defined by Eq. (18) performs the desired reshaping:

$$\begin{aligned} H_{\text{eff}} &= \mathbb{E}_{U \sim \mathcal{D}} U^\dagger H U = \frac{1}{2\pi} \int_0^{2\pi} d\theta e^{i\theta(n_1+n_2)} H e^{-i\theta(n_1+n_2)} \\ &= \omega_1 n_1 + \omega_2 n_2 + \omega_3 n_3 + \omega_4 n_4 + \xi_{12} n_1 n_2 + \xi_{34} n_3 n_4 \end{aligned} \quad (20)$$

As noted in [36] for the bosonic setting, the above reshaping can be interpreted as enforcing the U(1) symmetry of particle number conservation on the first spatial site of the system, comprising spin modes 1 and 2.

Notice that system modes 1 and 2 evolve independently from modes 3 and 4 in the dynamics generated by H_{eff} because no terms couple the two pairs. Therefore, if we could perform time evolution $\exp(-iH_{\text{eff}}t)$ generated by the reshaped Hamiltonian H_{eff} rather than the original Hamiltonian H , we could use robust phase estimation as described in Section 2.2 to learn the coefficients corresponding to the two sites in parallel, due to their decoupling. In practice, we will not be able to perform $\exp(-iH_{\text{eff}}t)$ exactly, but can approximate it by the following sequence of operators:

$$e^{-iH_{\text{eff}}t} \approx \prod_{j=1}^r U_j^\dagger e^{-iHt/r} U_j \quad (21)$$

where each U_j is independently sampled from the distribution \mathcal{D} . In the limit $r \rightarrow \infty$, the above time evolution approaches the desired time evolution $\exp(-iH_{\text{eff}}t)$. In Appendix 3, we discuss the following bound that holds for the expectation values of any operator O with finite ($\mathcal{O}(1)$) support and $\|O\| \leq 1$:

$$|\text{Tr}(\rho(t)_{\text{approx}}O) - \text{Tr}(\rho(t)_{\text{exact}}O)| \leq \mathcal{O}\left(\frac{t^2\lambda_{\text{max}}^2}{r}\right) \quad (22)$$

where

$$\rho(t)_{\text{approx}} = \mathbb{E}_{U_j \sim \mathcal{D}} \left(\prod_{1 \leq j \leq r}^{\leftarrow} U_j^\dagger e^{-iHt/r} U_j \right) \rho \left(\prod_{1 \leq j \leq r}^{\rightarrow} U_j^\dagger e^{iHt/r} U_j \right), \quad (23)$$

$\rho(t)_{\text{exact}} = e^{-iH_{\text{eff}}t} \rho e^{iH_{\text{eff}}t}$, and λ_{max} is the largest absolute value among the Hamiltonian coefficients, which we henceforth take to be 1.

The outcome probabilities p_0 and p_+ of the RPE experiments in Section 2.2 (Eq. (7), Eq. (8) and Eq. (14)) can manifestly be expressed as expectation values of projection operators, which have norm 1. So by Eq. (22), performing RPE with the approximate time evolution operator in Eq. (21) shifts the output probabilities by an additive error of magnitude $\mathcal{O}(\frac{t^2}{r})$. By choosing r such that this term is $\mathcal{O}(1)$ and sufficiently small, this additive error can be swept into the noise terms δ_0, δ_+ (c.f. Eq. (3)), and RPE can still be accurately performed.

Thus, performing RPE with the operator in Eq. (21), via the protocol described in Section 2.2, on the decoupled subsystems in parallel, allows us to learn ω_1 and ω_3 simultaneously with Heisenberg scaling. In fact, the procedure described above can be slightly simplified to achieve the same result. Currently, the unitaries $e^{-i\theta(n_1+n_2)}$ used for reshaping eliminate both sets of hopping terms in the original Hamiltonian of Eq. (15). This has the (approximate) effect of decoupling the first spatial site (modes 1 and 2) *completely* from the second spatial site (modes 3 and 4). This complete decoupling implies that we could equally well have chosen to learn ω_4 , rather than ω_3 , in parallel with ω_1 , by changing the ancilla coupling accordingly. But if we choose specifically to learn ω_1 and ω_3 in parallel, partial decoupling would suffice. In particular, instead of using the two-mode unitaries $e^{-i\theta(n_1+n_2)}$ for reshaping, we could use the single-mode unitaries $e^{-i\theta n_1}$ that only act on mode 1. This would eliminate the hopping terms $h_{13}a_1^\dagger a_3 + h_{31}a_3^\dagger a_1$ but not $h_{24}a_2^\dagger a_4 + h_{42}a_4^\dagger a_2$. Due to our choice of initial states described in Section 2.2, the latter pair of hopping terms would have no physical effect, since modes 2 and 4 would remain unoccupied throughout the experiment.

Next, to learn ω_2 and ω_4 , there are two approaches, as described in Section 2.2 for the single-site case. The approach with ancillae is analogous to the approach described above to learn ω_1 and ω_3 , in which case partial decoupling would suffice (that is, $e^{-i\theta n_2}$ can be used for reshaping, allowing $h_{13}a_1^\dagger a_3 + h_{31}a_3^\dagger a_1$ to remain in the Hamiltonian). On the other hand, in the ancilla-free approach, full decoupling is required – both sets of hopping terms must be effectively eliminated. If $h_{13}a_1^\dagger a_3 + h_{31}a_3^\dagger a_1$ remains in the reshaped Hamiltonian, this acts nontrivially on the states of the form in Eq. (10). The ancilla-free procedure described in Section 2.2 then no longer yields the desired measurement statistics. Hence, the ancilla-free approach requires reshaping with $e^{-i\theta(n_1+n_2)}$. To learn the coefficients ω_2 and ω_4 , we therefore have a tradeoff: the ancilla-based approach allows reshaping with single-mode unitaries at

the expense of ancillary modes, while the ancilla-free approach requires two-mode unitaries for reshaping but no ancillary resources.

Finally, to learn ξ_{12} and ξ_{34} , the procedure is almost identical to that used for ω_1 and ω_3 , except that ancillae are not involved. As in the single-site case of Section 2.2, the initial states are modified accordingly.

2.3.2 Learning coefficients of hopping terms

To learn the (generically complex) hopping amplitudes, h_{13} and h_{24} , we offer two approaches, one ancilla-dependent and the other ancilla-free. In both cases, we first perform a change of basis via a Bogoliubov transformation. In the new basis, the real or imaginary components of h_{13} and h_{24} appear as coefficients of number-conserving terms, enabling us to learn these parameters using the reshaping approach as in Section 2.3.1 above. We will need to use different basis transformations to learn the real and imaginary components. The basis transformations on modes 1 and 3 are defined by the two-mode FLO unitaries $U_x^{(1,3)}$ and $U_y^{(1,3)}$ (representing fermionic beamsplitter operations as in Eq. (9)):

$$\begin{aligned} U_x^{(1,3)}(\theta) &= e^{i\theta(a_1^\dagger a_3 + a_3^\dagger a_1)} = \mathbb{I} + (\cos \theta - 1)(n_1 - n_3)^2 + i \sin \theta (a_1^\dagger a_3 + a_3^\dagger a_1) \\ U_y^{(1,3)}(\theta) &= e^{\theta(a_1^\dagger a_3 - a_3^\dagger a_1)} = \mathbb{I} + (\cos \theta - 1)(n_1 - n_3)^2 - \sin \theta (a_1^\dagger a_3 - a_3^\dagger a_1). \end{aligned} \quad (24)$$

The annihilation operators a_1 and a_3 are transformed as follows:

$$\begin{aligned} \begin{pmatrix} U_x^{(1,3)}(\theta) a_1 U_x^{(1,3)\dagger}(\theta) \\ U_x^{(1,3)}(\theta) a_3 U_x^{(1,3)\dagger}(\theta) \end{pmatrix} &= \begin{pmatrix} \cos \theta & -i \sin \theta \\ -i \sin \theta & \cos \theta \end{pmatrix} \begin{pmatrix} a_1 \\ a_3 \end{pmatrix} \\ \begin{pmatrix} U_y^{(1,3)}(\theta) a_1 U_y^{(1,3)\dagger}(\theta) \\ U_y^{(1,3)}(\theta) a_3 U_y^{(1,3)\dagger}(\theta) \end{pmatrix} &= \begin{pmatrix} \cos \theta & \sin \theta \\ -\sin \theta & \cos \theta \end{pmatrix} \begin{pmatrix} a_1 \\ a_3 \end{pmatrix}. \end{aligned} \quad (25)$$

The basis transformations on modes 2 and 4 are given by the analogously defined unitaries $U_x^{(2,4)}$ and $U_y^{(2,4)}$. Comparing to the case of bosonic operators explored in [36], the U_x -transformation differs by a minus sign on the off-diagonal terms, while the U_y -transformation is identical.

In both the ancilla-based and the ancilla-free protocols, the hopping coefficients are learned in two steps. First, we use the U_y basis to learn the real components, $\text{Re}(h_{13})$ and $\text{Re}(h_{24})$; then we use the U_x basis to learn the imaginary components, $\text{Im}(h_{13})$ and $\text{Im}(h_{24})$.

Starting with the real components, consider the transformation obtained by simultaneously rotating all four modes using $U_y^{(1,3)}(\theta)$ and $U_y^{(2,4)}(\theta)$ at $\theta = \frac{\pi}{4}$. The transformed fermionic operators $\tilde{a}_1, \tilde{a}_2, \tilde{a}_3, \tilde{a}_4$ are given by

$$\begin{aligned} \begin{pmatrix} \tilde{a}_1 \\ \tilde{a}_3 \end{pmatrix} &= \begin{pmatrix} U_y^{(1,3)}(\frac{\pi}{4}) a_1 U_y^{\dagger(1,3)}(\frac{\pi}{4}) \\ U_y^{(1,3)}(\frac{\pi}{4}) a_3 U_y^{\dagger(1,3)}(\frac{\pi}{4}) \end{pmatrix} = \frac{1}{\sqrt{2}} \begin{pmatrix} 1 & 1 \\ -1 & 1 \end{pmatrix} \begin{pmatrix} a_1 \\ a_3 \end{pmatrix} \\ \begin{pmatrix} \tilde{a}_2 \\ \tilde{a}_4 \end{pmatrix} &= \begin{pmatrix} U_y^{(2,4)}(\frac{\pi}{4}) a_2 U_y^{\dagger(2,4)}(\frac{\pi}{4}) \\ U_y^{(2,4)}(\frac{\pi}{4}) a_4 U_y^{\dagger(2,4)}(\frac{\pi}{4}) \end{pmatrix} = \frac{1}{\sqrt{2}} \begin{pmatrix} 1 & 1 \\ -1 & 1 \end{pmatrix} \begin{pmatrix} a_2 \\ a_4 \end{pmatrix}. \end{aligned} \quad (26)$$

Under this basis change, our two-site Hamiltonian in Eq. (15) is transformed as follows:

$$\begin{aligned}
H \mapsto \tilde{H} &= \left(\frac{\omega_1 + \omega_3}{2} + \text{Re}(h_{13}) \right) \tilde{n}_1 + \left(\frac{\omega_2 + \omega_4}{2} + \text{Re}(h_{24}) \right) \tilde{n}_2 \\
&+ \left(\frac{\omega_1 + \omega_3}{2} - \text{Re}(h_{13}) \right) \tilde{n}_3 + \left(\frac{\omega_2 + \omega_4}{2} - \text{Re}(h_{24}) \right) \tilde{n}_4 \\
&+ \left(\frac{\xi_{12} + \xi_{34}}{4} \right) (\tilde{n}_1 \tilde{n}_2 + \tilde{n}_2 \tilde{n}_3 + \tilde{n}_3 \tilde{n}_4 + \tilde{n}_1 \tilde{n}_4) \\
&+ \left(\frac{\omega_3 - \omega_1}{2} \right) (\tilde{a}_1^\dagger \tilde{a}_3 + \tilde{a}_3^\dagger \tilde{a}_1) + \left(\frac{\omega_4 - \omega_2}{2} \right) (\tilde{a}_2^\dagger \tilde{a}_4 + \tilde{a}_4^\dagger \tilde{a}_2) \\
&+ \left(\frac{\xi_{34} - \xi_{12}}{4} \right) ((\tilde{n}_1 + \tilde{n}_3) (\tilde{a}_2^\dagger \tilde{a}_4 + \tilde{a}_4^\dagger \tilde{a}_2) + (\tilde{n}_2 + \tilde{n}_4) (\tilde{a}_1^\dagger \tilde{a}_3 + \tilde{a}_3^\dagger \tilde{a}_1)) \\
&+ \left(\frac{\xi_{12} + \xi_{34}}{4} \right) (\tilde{a}_1^\dagger \tilde{a}_3 + \tilde{a}_3^\dagger \tilde{a}_1) (\tilde{a}_2^\dagger \tilde{a}_4 + \tilde{a}_4^\dagger \tilde{a}_2).
\end{aligned} \tag{27}$$

It is evident from this expression that learning the coefficients of \tilde{n}_1 and \tilde{n}_2 in \tilde{H} (that is, the coefficients of the first two terms in Eq. (27)) is sufficient to learn $\text{Re}(h_{13})$ and $\text{Re}(h_{24})$, assuming $\omega_1, \omega_2, \omega_3$ and ω_4 have already been learned using the technique of Section 2.3.1.

To learn the desired parameters of \tilde{H} , we will apply the reshaping technique as in Section 2.3.1, but in the U_y -basis. In this case, the distribution \mathcal{D} used for reshaping is defined by unitaries of the form $e^{-i\theta(\tilde{n}_1 + \tilde{n}_2)}$ with $\theta \sim \mathcal{U}([0, 2\pi])$. Note that these number-preserving operators in the U_y -basis can be expressed in terms of the U_x operators introduced in Eq. (24),

$$\begin{aligned}
e^{i\theta\tilde{n}_1} &= e^{i\frac{\theta}{2}(n_1+n_3)} U_x^{(1,3)}\left(\frac{\theta}{2}\right) \\
e^{i\theta\tilde{n}_2} &= e^{i\frac{\theta}{2}(n_2+n_4)} U_x^{(2,4)}\left(\frac{\theta}{2}\right).
\end{aligned} \tag{28}$$

So, defining $U_x(\theta) = U_x^{(1,3)}(\theta)U_x^{(2,4)}(\theta)$, we have $e^{i\theta(\tilde{n}_1 + \tilde{n}_2)} = e^{i\frac{\theta}{2}(n_1+n_2+n_3+n_4)} U_x(\frac{\theta}{2})$. Since the total number of particles across all four modes, $n_1 + n_2 + n_3 + n_4$, is conserved by the Hamiltonian H , conjugation by $e^{-i\theta(\tilde{n}_1 + \tilde{n}_2)}$ is equivalent to conjugation by $U_x(\theta)$:

$$e^{i\theta(\tilde{n}_1 + \tilde{n}_2)} H e^{-i\theta(\tilde{n}_1 + \tilde{n}_2)} = U_x\left(\frac{\theta}{2}\right) H U_x\left(-\frac{\theta}{2}\right). \tag{29}$$

So averaging over the distribution \mathcal{D} is equivalent to averaging over $U_x(\frac{\theta}{2})$ with $\theta \sim \mathcal{U}([0, 2\pi])$.

From the properties of fermionic operators listed in Eq. (19), it follows that conjugation of \tilde{H} by $U \sim \mathcal{D}$ cancels, in expectation, the terms that are not particle-number conserving in either of the first two modes (in the U_y -basis). This leaves the following reshaped Hamiltonian:

$$\begin{aligned}
\tilde{H}_{\text{eff}} &= \mathbb{E}_{U \sim \mathcal{D}} U^\dagger \tilde{H} U = \frac{1}{2\pi} \int_0^{2\pi} d\theta e^{i\theta(\tilde{n}_1 + \tilde{n}_2)} H e^{-i\theta(\tilde{n}_1 + \tilde{n}_2)} = \frac{1}{2\pi} \int_0^{2\pi} d\theta U_x\left(\frac{\theta}{2}\right) H U_x\left(-\frac{\theta}{2}\right) \\
&= \left(\frac{\omega_1 + \omega_3}{2} + \text{Re}(h_{13}) \right) \tilde{n}_1 + \left(\frac{\omega_2 + \omega_4}{2} + \text{Re}(h_{24}) \right) \tilde{n}_2 \\
&+ \left(\frac{\omega_1 + \omega_3}{2} - \text{Re}(h_{13}) \right) \tilde{n}_3 + \left(\frac{\omega_2 + \omega_4}{2} - \text{Re}(h_{24}) \right) \tilde{n}_4 \\
&+ \left(\frac{\xi_{12} + \xi_{34}}{4} \right) (\tilde{n}_1 \tilde{n}_2 + \tilde{n}_2 \tilde{n}_3 + \tilde{n}_3 \tilde{n}_4 + \tilde{n}_1 \tilde{n}_4).
\end{aligned} \tag{30}$$

As in Section 2.3.1, in practice we will use an approximate version of the time evolution operator corresponding to the reshaped Hamiltonian, obtained by sampling a finite number of unitaries from \mathcal{D} :

$$\prod_{j=1}^r U_x\left(\frac{\theta_j}{2}\right) e^{-iHt/r} U_x\left(-\frac{\theta_j}{2}\right) \quad (31)$$

Now, to perform RPE, we can proceed either with an ancilla or without.

Learning hopping coefficients: ancilla-based protocol

A single ancilla is used to learn the coefficients of \tilde{n}_1 and \tilde{n}_2 in turn. To specify the RPE protocol, we need analogues of the states $V(-\frac{\pi}{4})|\Omega\rangle$ and $W(-\frac{\pi}{4})|\Omega\rangle$ that appeared in the single-site protocol (Eq. (5) of Section 2.2), in the U_y -basis. Using b^\dagger to denote the creation operator for the ancilla mode, the required states are given by

$$\begin{aligned} U_y^{(1,3)}\left(\frac{\pi}{4}\right)V\left(-\frac{\pi}{4}\right)|\Omega\rangle &= \frac{1}{\sqrt{2}}(|\Omega\rangle + \tilde{a}_1^\dagger b^\dagger |\Omega\rangle) \\ U_y^{(1,3)}\left(\frac{\pi}{4}\right)W\left(-\frac{\pi}{4}\right)|\Omega\rangle &= \frac{1}{\sqrt{2}}(|\Omega\rangle - i\tilde{a}_1^\dagger b^\dagger |\Omega\rangle) \end{aligned} \quad (32)$$

where $V(-\frac{\pi}{4})|\Omega\rangle$ and $W(-\frac{\pi}{4})|\Omega\rangle$ are the same two-mode operators introduced in Eq. (4), which act on system mode 1 (in the original basis) and the ancilla mode. Eq. (32) can be easily derived using the properties $\tilde{a}_1^\dagger U_y^{(1,3)}\left(\frac{\pi}{4}\right) = U_y^{(1,3)}\left(\frac{\pi}{4}\right)a_1^\dagger$ and $U_y^{(1,3)}\left(\frac{\pi}{4}\right)|\Omega\rangle = |\Omega\rangle$.

Having defined these states, the rest of the procedure is completely analogous to that used to learn ω_1 in Section 2.2, with time evolution being generated by the approximate operator in Eq. (31). For the Type-0 experiment, apply the following sequence of operators to the initial state:

$$V^\dagger\left(-\frac{\pi}{4}\right)U_y^{\dagger(1,3)}\left(\frac{\pi}{4}\right)\left(\prod_{j=1}^r U_x\left(\frac{\theta_j}{2}\right) e^{-iHt/r} U_x\left(-\frac{\theta_j}{2}\right)\right)U_y^{(1,3)}\left(\frac{\pi}{4}\right)V\left(-\frac{\pi}{4}\right)|\Omega\rangle. \quad (33)$$

After measuring the occupation of system mode 1 and the ancilla, the probability of returning to the vacuum state is given by

$$\begin{aligned} p_0 &= |\langle\Omega|V^\dagger\left(-\frac{\pi}{4}\right)U_y^{\dagger(1,3)}\left(\frac{\pi}{4}\right)\left(\prod_{j=1}^r U_x\left(\frac{\theta_j}{2}\right) e^{-iHt/r} U_x\left(-\frac{\theta_j}{2}\right)\right)U_y^{(1,3)}\left(\frac{\pi}{4}\right)V\left(-\frac{\pi}{4}\right)|\Omega\rangle|^2 \\ &= \frac{1}{2}\left(1 + \cos\left(\frac{\omega_1 + \omega_3}{2} + \text{Re}(h_{13})\right)\right) + \delta_0 \end{aligned} \quad (34)$$

where the constant additive error δ_0 comprises the approximation error in the time evolution operator and SPAM error. For the Type-+ experiment, apply a similar sequence of operators to the initial state, but with $V^\dagger(-\frac{\pi}{4})$ replaced by $W^\dagger(-\frac{\pi}{4})$:

$$W^\dagger\left(-\frac{\pi}{4}\right)U_y^{\dagger(1,3)}\left(\frac{\pi}{4}\right)\left(\prod_{j=1}^r U_x\left(\frac{\theta_j}{2}\right) e^{-iHt/r} U_x\left(-\frac{\theta_j}{2}\right)\right)U_y^{(1,3)}\left(\frac{\pi}{4}\right)V\left(-\frac{\pi}{4}\right)|\Omega\rangle \quad (35)$$

Then the probability of returning to the vacuum state upon measurement is given by

$$\begin{aligned}
p_+ &= |\langle \Omega | W^\dagger(-\frac{\pi}{4}) U_y^{\dagger(1,3)}(\frac{\pi}{4}) \left(\prod_{j=1}^r U_x\left(\frac{\theta_j}{2}\right) e^{-iHt/r} U_x\left(-\frac{\theta_j}{2}\right) \right) U_y^{(1,3)}(\frac{\pi}{4}) V(-\frac{\pi}{4}) | \Omega \rangle|^2 \\
&= \frac{1}{2} \left(1 + \sin\left(\frac{\omega_1 + \omega_3}{2} + \text{Re}(h_{13})\right) \right) + \delta_+.
\end{aligned} \tag{36}$$

As before, these experiments are run for varying amounts of time evolution and repetitions in accordance with the RPE procedure, to generate an estimate of $\frac{\omega_1 + \omega_3}{2} + \text{Re}(h_{13})$ with Heisenberg scaling. Using the previously obtained estimates of ω_1 and ω_3 , this yields an estimate of $\text{Re}(h_{13})$. Appendix 3 justifies the use of linear combinations of estimators in this way, even though the estimates of ω_1 and ω_3 are not truly independent (having been learned in parallel with approximate, rather than exact, decoupling of modes 1 and 3).

As noted in the single site case of Section 2.2, one possible benefit of the ancilla-based protocol over the ancilla-free one is that, due to the mode occupancies of the initial state, modes 2 and 4 are effectively passive throughout the experiment. So reshaping with $U_x(\frac{\theta}{2})$ (equivalent to reshaping with $e^{i\theta(\tilde{n}_1 + \tilde{n}_2)}$ by Eq. (28)) is not actually necessary. Partial decoupling using $U_x^{(1,3)}(\frac{\theta}{2})$ (equivalent to using $e^{i\theta\tilde{n}_1}$) would suffice. The latter is a two-mode unitary acting on modes 1 and 3. On the other hand, $U_x(\frac{\theta}{2}) = U_x^{(1,3)}(\frac{\theta}{2}) U_x^{(2,4)}(\frac{\theta}{2})$, is a product of two-mode unitaries, collectively acting on all four modes, which might be less preferable to implement in certain experimental setups. In the ancilla-free protocol, this choice is not available; we will see shortly that reshaping must be performed with the full $U_x(\frac{\theta}{2})$ operator in that approach.

To learn the coefficient of \tilde{n}_2 using the ancilla, the protocol is analogous, with operators $V(-\frac{\pi}{4})$ and $W(-\frac{\pi}{4})$ now acting on system mode 2 and the ancilla:

$$\begin{aligned}
V(\theta) &= e^{\theta(a_2^\dagger b^\dagger - b a_2)} \\
W(\theta) &= e^{i\theta(a_2^\dagger b^\dagger + b a_2)}.
\end{aligned} \tag{37}$$

The initial state is $U_y^{(2,4)}(\frac{\pi}{4}) V(-\frac{\pi}{4}) | \Omega \rangle = \frac{1}{\sqrt{2}} (| \Omega \rangle + \tilde{a}_2^\dagger b^\dagger | \Omega \rangle)$. Running RPE yields an estimate of $\text{Re}(h_{24})$, assuming ω_2 and ω_4 have been previously estimated.

Learning hopping coefficients: ancilla-free protocol

Alternatively, to learn $\text{Re}(h_{13})$ and $\text{Re}(h_{24})$ without the ancilla, we utilize not just the previously estimated chemical potentials $\omega_1, \dots, \omega_4$, but also the on-site interaction coefficients ξ_{12} and ξ_{34} . By using two different initial states, we can estimate linear combinations of these eight parameters, from which estimates of $\text{Re}(h_{13})$ and $\text{Re}(h_{24})$ can be extracted.

For the first round of experiments, we use slightly modified versions of the operators $V(-\frac{\pi}{4})$ and $W(-\frac{\pi}{4})$ defined in Eq. (4), now acting on system modes 1 and 2:

$$\begin{aligned}
V(\theta) &= e^{\theta(a_1^\dagger a_2^\dagger - a_2 a_1)} \\
W(\theta) &= e^{i\theta(a_1^\dagger a_2^\dagger + a_2 a_1)}.
\end{aligned} \tag{38}$$

Defining $U_y(\theta) = U_y^{(1,3)}(\theta) U_y^{(2,4)}(\theta)$, the initial state used is $U_y(\frac{\pi}{4})V(-\frac{\pi}{4})|\Omega\rangle = \frac{1}{\sqrt{2}}(|\Omega\rangle + \tilde{a}_1^\dagger \tilde{a}_2^\dagger |\Omega\rangle)$. In this ancilla-free setting, reshaping must be performed with $U_x(\frac{\theta}{2})$ to ensure that all hopping terms are eliminated. Defining $p = \frac{\omega_1 + \omega_3}{2}$, $q = \frac{\omega_2 + \omega_4}{2}$, and $r = \frac{\xi_{12} + \xi_{34}}{4}$, the Type-0 success probability (that of obtaining the vacuum state upon measurement) is given by

$$\begin{aligned} p_0 &= |\langle \Omega | V^\dagger(-\frac{\pi}{4}) U_y^\dagger(\frac{\pi}{4}) \left(\prod_{j=1}^r U_x\left(\frac{\theta_j}{2}\right) e^{-iHt/r} U_x\left(-\frac{\theta_j}{2}\right) \right) U_y(\frac{\pi}{4}) V(-\frac{\pi}{4}) |\Omega\rangle|^2 \\ &= \frac{1}{2} \left(1 + \cos(p + q + r + \text{Re}(h_{13}) + \text{Re}(h_{24})) \right) + \delta_0 \end{aligned} \quad (39)$$

The Type-+ success probability is given by

$$\begin{aligned} p_+ &= |\langle \Omega | W^\dagger(-\frac{\pi}{4}) U_y^\dagger(\frac{\pi}{4}) \left(\prod_{j=1}^r U_x\left(\frac{\theta_j}{2}\right) e^{-iHt/r} U_x\left(-\frac{\theta_j}{2}\right) \right) U_y(\frac{\pi}{4}) V(-\frac{\pi}{4}) |\Omega\rangle|^2 \\ &= \frac{1}{2} \left(1 + \sin(p + q + r + \text{Re}(h_{13}) + \text{Re}(h_{24})) \right) + \delta_+. \end{aligned} \quad (40)$$

Using RPE, these experiments provide an estimate of $(p + q + r + \text{Re}(h_{13}) + \text{Re}(h_{24}))$.

For the next round of experiments, we use different initial states and final measurement bases. To define them, we use the operators $V'(-\frac{\pi}{4})$ and $W'(-\frac{\pi}{4})$ defined in Eq. (9). The initial state for RPE is $U_y(\frac{\pi}{4})V'(-\frac{\pi}{4})(a_1^\dagger |\Omega\rangle) = \frac{1}{\sqrt{2}}(\tilde{a}_1^\dagger |\Omega\rangle + \tilde{a}_2^\dagger |\Omega\rangle)$. This is analogous to the state used in the ancilla-free approach to learning ω_2 in Section 2.2 (the state in the first line of Eq. (10)), but in the U_y -basis. Reshaping with $U_x(\frac{\theta}{2})$ and applying $V'^\dagger(-\frac{\pi}{4})U_y^\dagger(\frac{\pi}{4})$ before measurement, the Type-0 success probability (that of obtaining $a_1^\dagger |\Omega\rangle$ upon measurement) is given by:

$$\begin{aligned} p_0 &= |(\langle \Omega | a_1) V'^\dagger(-\frac{\pi}{4}) U_y^\dagger(\frac{\pi}{4}) \left(\prod_{j=1}^r U_x\left(\frac{\theta_j}{2}\right) e^{-iHt/r} U_x\left(-\frac{\theta_j}{2}\right) \right) U_y(\frac{\pi}{4}) V'(-\frac{\pi}{4}) (a_1^\dagger |\Omega\rangle)|^2 \\ &= \frac{1}{2} \left(1 + \cos(\text{Re}(h_{24}) - \text{Re}(h_{13}) + q - p) \right) + \delta_0 \end{aligned} \quad (41)$$

Similarly, applying $W'^\dagger(-\frac{\pi}{4})U_y^\dagger(\frac{\pi}{4})$ before measurement, the Type-+ success probability is given by

$$\begin{aligned} p_+ &= |(\langle \Omega | a_1) W'^\dagger(-\frac{\pi}{4}) U_y^\dagger(\frac{\pi}{4}) \left(\prod_{j=1}^r U_x\left(\frac{\theta_j}{2}\right) e^{-iHt/r} U_x\left(-\frac{\theta_j}{2}\right) \right) U_y(\frac{\pi}{4}) V'(-\frac{\pi}{4}) (a_1^\dagger |\Omega\rangle)|^2 \\ &= \frac{1}{2} \left(1 + \sin(\text{Re}(h_{24}) - \text{Re}(h_{13}) + q - p) \right) + \delta_+. \end{aligned} \quad (42)$$

Using RPE, these experiments provide an estimate of $(\text{Re}(h_{24}) - \text{Re}(h_{13}) + q - p)$.

Now, using the previous estimates of $\omega_1, \omega_2, \omega_3, \omega_4, \xi_{12}$ and ξ_{34} , we have estimates of p, q and r . By taking the appropriate linear combinations of our newly obtained estimates for $(p + q + r + \text{Re}(h_{13}) + \text{Re}(h_{24}))$ and $(\text{Re}(h_{24}) - \text{Re}(h_{13}) + q - p)$, we can estimate $\text{Re}(h_{13})$ and $\text{Re}(h_{24})$.

This concludes the discussion of the two approaches to learning the real components, $\text{Re}(h_{13})$ and $\text{Re}(h_{24})$, of the hopping coefficients. Finally, to learn the imaginary components $\text{Im}(h_{13})$ and $\text{Im}(h_{24})$, we can use the same procedures as for the real components, but with the roles of U_x and U_y interchanged. The transformed fermionic operators $\tilde{a}_1, \tilde{a}_2, \tilde{a}_3, \tilde{a}_4$ in this case are given by

$$\begin{aligned} \begin{pmatrix} \tilde{a}_1 \\ \tilde{a}_3 \end{pmatrix} &= \begin{pmatrix} U_x^{(1,3)}(\frac{\pi}{4}) a_1 U_x^{\dagger(1,3)}(\frac{\pi}{4}) \\ U_x^{(1,3)}(\frac{\pi}{4}) a_3 U_x^{\dagger(1,3)}(\frac{\pi}{4}) \end{pmatrix} = \frac{1}{\sqrt{2}} \begin{pmatrix} 1 & -i \\ -i & 1 \end{pmatrix} \begin{pmatrix} a_1 \\ a_3 \end{pmatrix} \\ \begin{pmatrix} \tilde{a}_2 \\ \tilde{a}_4 \end{pmatrix} &= \begin{pmatrix} U_x^{(2,4)}(\frac{\pi}{4}) a_2 U_x^{\dagger(2,4)}(\frac{\pi}{4}) \\ U_x^{(2,4)}(\frac{\pi}{4}) a_4 U_x^{\dagger(2,4)}(\frac{\pi}{4}) \end{pmatrix} = \frac{1}{\sqrt{2}} \begin{pmatrix} 1 & -i \\ -i & 1 \end{pmatrix} \begin{pmatrix} a_2 \\ a_4 \end{pmatrix}. \end{aligned} \quad (43)$$

The basis-transformed Hamiltonian has a similar form as Eq. (27), with the coefficient of \tilde{n}_1 being $\frac{\omega_1 + \omega_3}{2} - \text{Im}(h_{13})$ and the coefficient of \tilde{n}_2 being $\frac{\omega_2 + \omega_4}{2} - \text{Im}(h_{24})$, hence it suffices to learn these two coefficients. The unitaries used to reshape the Hamiltonian can be expressed in terms of $U_y(\theta) = U_y^{(1,3)}(\theta) U_y^{(2,4)}(\theta)$, observing that $e^{i\theta(\tilde{n}_1 + \tilde{n}_2)} = e^{i\frac{\theta}{2}(n_1 + n_2 + n_3 + n_4)} U_y(\frac{\theta}{2})$. The rest of the procedure, whether ancilla-based or ancilla-free, is analogous to the procedure for the real components.

2.4 Learning a many-body Hamiltonian

Having considered the single-site and two-site cases, we finally come to the N -site many-body Hamiltonians of interest:

$$H = \sum_{\langle i,j \rangle} \sum_{\sigma \in \{\uparrow, \downarrow\}} h_{ij\sigma} a_{i\sigma}^\dagger a_{j\sigma} + \sum_{\sigma \in \{\uparrow, \downarrow\}} \omega_{i\sigma} n_{i\sigma} + \sum_i \xi_i n_{i\uparrow} n_{i\downarrow}. \quad (44)$$

As in Section 2.1, we are now explicitly indexing the *spatial* sites by i, j , and distinguishing the two spin modes at each site by \uparrow and \downarrow . Pairs of spatial sites coupled by a hopping interaction are denoted by $\langle i, j \rangle$. We can associate each spatial site to a vertex of a graph G , with edges between sites coupled by a hopping interaction. We assume that the degree of each vertex is $\mathcal{O}(1)$.

Hamiltonians of this form can be learned using the same divide-and-conquer strategy used for many-body qubit Hamiltonians [35] and bosonic Hamiltonians [36]. The key idea is that the decoupling technique used to eliminate hopping terms in the two-site case (Section 2.3) can be used to decouple the Hamiltonian in Eq. (44) into multiple non-interacting clusters, whose parameters can be learned in parallel. The learning problem is then effectively reduced to the two-site case.

To perform the decoupling, we start with the graph $G = (V, E)$ of fermionic sites. V is the set of vertices (representing spatial fermionic sites) and E is the set of edges. Using the terminology of [36], consider the *link graph*, $L = (E, E_L)$. The set of vertices of the link graph L is the set E of edges of the original graph G , so each vertex of L represents a pair $\langle i, j \rangle$ of spatial sites coupled by a hopping interaction. There is an edge between two vertices of L if and only if the corresponding edges in the original graph G intersect at a vertex. In other words, the interactions that they represent involve a common spatial site. The link

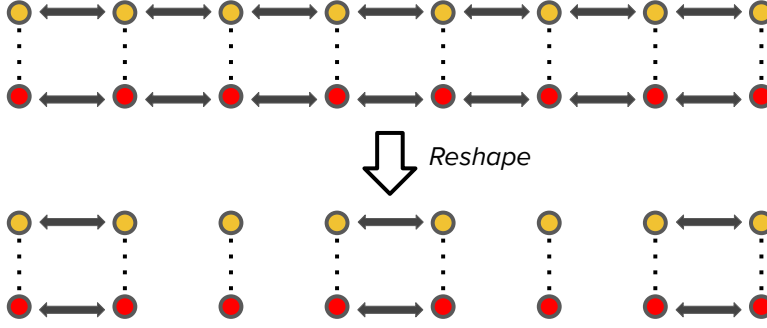


Figure 4: By effectively eliminating a subset of the hopping interactions, reshaping decouples the system into independent two-site (four-mode) clusters that can be learned in parallel using the techniques of Section 2.3. This figure depicts reshaping for the special case of a one-dimensional lattice.

graph L can be viewed as the analogue of the *dual interaction graph* of qubit Hamiltonians [29, 35].

The link graph L is used to partition the Hamiltonian into clusters that can be decoupled. Specifically, consider a coloring of L such that each vertex is a different color from all its neighbors and next-nearest neighbors. The number of colors needed is χ . As noted in [36], $\chi \leq 4(\deg(G) - 1)^2 + 1$, and such a coloring can be found by a greedy algorithm. The coloring partitions the vertices of L into disjoint sets E_c , each labelled by a different color $c \in \{1, \dots, \chi\}$.

For each color c , the goal is to reshape the Hamiltonian such that the interactions $E \setminus E_c$ are eliminated. That is, the only surviving interactions are the ones represented by E_c . As in Section 2.3, this can be achieved by conjugating the Hamiltonian by suitably distributed random unitaries. Let V_c be the set of spatial sites (vertices of G) involved in the interactions represented by E_c . The unitaries used for reshaping have the form

$$\prod_{j \in V \setminus V_c} e^{-i\theta_j(n_{j\uparrow} + n_{j\downarrow})} \quad (45)$$

with each $\theta_j \sim \mathcal{U}([0, 2\pi])$. By similar calculations to those used in Section 2.3, one can check that the Hamiltonian obtained by conjugating with the unitaries above eliminates, in expectation, all but those interactions contained in E_c :

$$H = \sum_{\langle i, j \rangle \in E_c} \sum_{\sigma \in \{\uparrow, \downarrow\}} h_{ij\sigma} a_{i\sigma}^\dagger a_{j\sigma} + \sum_{\sigma \in \{\uparrow, \downarrow\}} \omega_{i\sigma} n_{i\sigma} + \sum_i \xi_i n_{i\uparrow} n_{i\downarrow} \quad (46)$$

Furthermore, by construction (due to the coloring rules for the link graph), each pair of interacting vertices $\langle i, j \rangle$ in the reshaped Hamiltonian has no overlap with any other pair of interacting vertices. Thus, the reshaped Hamiltonian is a sum of decoupled two-site Hamiltonians, which can be learned in parallel using the approach described in Section 2.3. In fact, as explained in Section 2.2 and Section 2.3, some of the unitaries in Eq. (45) can be replaced by either $e^{-i\theta_j n_{j\uparrow}}$ or $e^{-i\theta_j n_{j\downarrow}}$ in the ancilla-based protocols, depending on which

coefficient is to be learned. We can ignore the terms $\omega_{i\sigma}n_{i\sigma}$ and $\xi_i n_{i\uparrow}n_{i\downarrow}$ for $i \in V \setminus V_c$ in the reshaped Hamiltonian, since they have no effect due to our choice of initial states.

Repeating this process for each one of the χ -many colors c results in learning all the parameters of the original Hamiltonian. Therefore, the time complexity overhead compared to the two-site case is a multiplicative factor of χ . Since the graph G has bounded degree, χ and hence the time complexity of the procedure remains $\mathcal{O}(1/\varepsilon)$, independent of the number of fermionic sites N . To implement ancilla-based protocols for any given any color, two ancillae are needed for each of the $\mathcal{O}(N)$ two-mode subsystems being learned in parallel, leading to an overhead of $\mathcal{O}(N)$ ancillae. The ancillae can be re-used across multiple experiments, so the ancilla count does not depend on the number of experimental rounds or number of colors.

To summarize the conceptual structure of the entire protocol:

1. Use a coloring of the link graph defined above to determine which two-site clusters can be learned in parallel. That is, determine which hopping interactions are to be eliminated by reshaping in order to obtain effectively independent two-site clusters. Each set of independent clusters corresponds to one of the colors used in the graph coloring. (The coloring is used to identify the appropriate unitary distribution for reshaping. The reshaping itself occurs during time evolution in each experiment, by inserting unitaries sampled from this distribution after sufficiently small time-steps of Hamiltonian evolution, as explained in Section 2.3).
2. For each color, learn the Hamiltonian parameters for all the independent two-site clusters in parallel, by performing the following sequence of steps on each cluster (comprising spatial sites i and j):
 - (a) Learn $\omega_{i\uparrow}$ and $\omega_{j\uparrow}$ in parallel (two ancillae required), as described in Section 2.3.1.
 - (b) Learn $\omega_{i\downarrow}$ and $\omega_{j\downarrow}$ in parallel (ancillae optional), as described in Section 2.3.1.
 - (c) Learn ξ_i and ξ_j in parallel (no ancillae), as described in Section 2.3.1.
 - (d) Learn $\text{Re}(h_{ij\uparrow})$ and $\text{Re}(h_{ij\downarrow})$ either sequentially (one ancilla required) or in parallel (no ancillae), as described in Section 2.3.2.
 - (e) Learn $\text{Im}(h_{ij\uparrow})$ and $\text{Im}(h_{ij\downarrow})$ either sequentially (one ancilla required) or in parallel (no ancillae), as described in Section 2.3.2.

3 Discussion

In this paper, we have addressed the problem of learning a class of fermionic Hubbard Hamiltonians of physical interest, with complex hopping amplitudes, nonzero chemical potentials, and on-site interactions. We have shown that the parameters of such Hamiltonians can be learned at the Heisenberg limit, where the total evolution time across all experiments is $\mathcal{O}(1/\varepsilon)$ and the number of experiments is $\mathcal{O}(\text{polylog}(1/\varepsilon))$, as long as the graph representing the fermionic interactions has bounded degree. Each experiment involves preparing fermionic Gaussian states, alternating time evolution with fermionic linear optics (FLO) unitaries according to the paradigm of discrete quantum control, performing local occupation number

measurements on the fermionic modes, and classically post-processing the results according to the Robust Phase Estimation algorithm [43–45]. Some of the experiments utilize $\mathcal{O}(N)$ fermionic ancilla modes, where N is the system size, to satisfy the constraints imposed by the parity superselection rule for fermions. The protocol is robust to a constant amount of state preparation and measurement error.

We saw that for certain steps of the protocol, the use of ancillae is optional, but provides a tradeoff in terms of resources. To learn some of the chemical potential terms, the ancillae enable discrete quantum control to be effective with single-mode FLO unitaries instead of two-mode FLO unitaries. In more physical terms, this means that ancillae allow trading two-mode fermionic phase-shifters for single-mode phase-shifters. While learning the hopping coefficients, ancillae enable the use of two-mode unitaries rather than a product of two-mode unitaries on non-overlapping modes – in other words, trading two beamsplitters for a single beamsplitter. The use of ancillae, for those steps of the protocol where they are optional, may therefore depend on which operations are easier to implement on a given platform. It’s easy to imagine other minor variations on the approach presented here that would also achieve the Heisenberg limit. For application to a specific platform, there is flexibility to tune the protocol to use the operations most easily implemented there.

A natural next step would be to find a Heisenberg-limited algorithm for our class of fermionic Hubbard Hamiltonians that eliminates the ancilla overhead altogether, for instance by learning appropriate linear combinations of the Hamiltonian parameters from which the individual parameters can be inferred. Furthermore, although both the bosonic Hamiltonians considered in [36] and the fermionic Hamiltonians considered here are physically well-motivated, they are still special cases of the larger set of physically interesting Hamiltonians. For instance, one could consider Hamiltonians that include mix bosonic, fermionic and qubit sites, such as the Bose-Fermi Hubbard model [65] and the Jaynes-Cummings model [66]. An interesting next step would be to investigate whether Heisenberg-limited learning is achievable for such Hamiltonians. More generally, however, it would be desirable to have a simple criterion, applying to a wide range of Hamiltonians, that serves as a sufficient condition for Heisenberg-limited learning to be possible. This is the case for qubit Hamiltonians [35, 37], where the relevant criterion is that the Hamiltonian is low-intersection. This criterion encompasses a larger set of qubit Hamiltonians compared to the more restricted classes of bosonic and fermionic Hamiltonians for which Heisenberg-limited learning algorithms have been established. A useful next step would therefore be to identify an assumption analogous to the low-intersection assumption, to extend these results to a wider set of bosonic and fermionic Hamiltonians.

Acknowledgments

We thank Vedika Khemani, Sri Raghu and Nicole Ticea for discussions on the Hubbard model, Di Fang, Jeongwan Haah and Yu Tong for discussions about qubit Hamiltonian learning algorithms, and Lexing Ying for introducing us to the bosonic case. This work was supported by the Herb and Jane Dwight Stanford Graduate Fellowship, ARO (award W911NF2120214), DOE (Q-NEXT), CIFAR and the Simons Foundation.

Appendix A: Analysis of reshaping error

In this section, we consider in more detail the error due to the approximate time evolution operator obtained via the reshaping procedure, introduced in Section 2.3.1:

$$\prod_{j=1}^r U_j^\dagger e^{-iHt/r} U_j \quad (47)$$

We wish to demonstrate that the following bound holds for the expectation values of any operator O_S with support on an $\mathcal{O}(1)$ subset S of fermionic modes and $\|O_S\| \leq 1$:

$$|\mathrm{Tr}(\rho(t)_{\mathrm{approx}} O_S) - \mathrm{Tr}(\rho(t)_{\mathrm{exact}} O_S)| \leq \mathcal{O}\left(\frac{t^2}{r}\right) \quad (48)$$

where

$$\rho(t)_{\mathrm{approx}} = \mathbb{E}_{U_j \sim \mathcal{D}} \left(\prod_{1 \leq j \leq r}^{\leftarrow} U_j^\dagger e^{-iHt/r} U_j \right) \rho \left(\prod_{1 \leq j \leq r}^{\rightarrow} U_j^\dagger e^{iHt/r} U_j \right), \quad (49)$$

and $\rho(t)_{\mathrm{exact}} = e^{-iH_{\mathrm{eff}}t} \rho e^{iH_{\mathrm{eff}}t}$. Here $H_{\mathrm{eff}} = \mathbb{E}_{U \sim \mathcal{D}} U^\dagger H U = H'_S + H'_{S^c}$, that is, the effective Hamiltonian decouples the original Hamiltonian into a sum of a Hamiltonian supported on S and a Hamiltonian supported on the rest of the system S^c . O_S acts nontrivially only on the modes in S , and acts implicitly as the identity operator on the other modes.

The outcome probabilities p_0 and p_+ of the various RPE experiments outlined in Section 2.3 can manifestly be expressed as expectation values of projection operators, which have norm 1 and act on at most four modes. Hence these projectors satisfy the requirements for the operators O_S in Eq. (48), and Eq. (48) justifies the use of the approximate time evolution operator in Eq. (47) for the RPE experiments. Throughout this section we set the largest absolute value among the Hamiltonian coefficients, $\lambda_{\max} = 1$. (For any other finite value, all the complexities in this section would simply pick up a constant multiplicative factor of λ_{\max}^2).

The bound in Eq. (47) is a corollary of the following bound originally derived for the special case of qubit Hamiltonians by Huang et al. [35]:

$$\left\| \mathbb{E}_{U_j \sim \mathcal{D}} \left(\prod_{1 \leq j \leq r}^{\rightarrow} U_j^\dagger e^{iHt/r} U_j \right) O_S \left(\prod_{1 \leq j \leq r}^{\leftarrow} U_j^\dagger e^{-iHt/r} U_j \right) - e^{iH_{\mathrm{eff}}t} O_S e^{-iH_{\mathrm{eff}}t} \right\| \leq \mathcal{O}\left(\frac{t^2}{r}\right) \quad (50)$$

Since $H_{\mathrm{eff}} = H'_S + H'_{S^c}$ and O_S acts nontrivially only on S , the H'_{S^c} term does not contribute to the Heisenberg-picture evolution of O_S . Hence the second term on the left hand side of Eq. (50) represents the ideal subsystem projector for RPE that acts nontrivially only on S , while the first term is the approximate projector that appears in the actual protocol.

As observed by [46], the proof of Eq. (50) in [35] applies to more general unitaries than the tensor products of Pauli operators considered in [35], including those relevant for the protocol of [46] and our protocol in this paper. Hence Eq. (50) can be proved analogously to the proof technique used in [35].

Appendix B: Root-mean-square error of linear combination of estimators

In each of the ancilla-free protocols described in Section 2, the RPE procedure does not directly yield an estimate of the desired parameter. Rather, it estimates a linear combination of the desired parameter and other parameters that have previously been estimated. We then estimate the desired parameter by appropriately adding or subtracting the previously obtained estimators of the other parameters in the linear combination. This process is straightforward when the estimators being linearly combined are obtained from different experiments and therefore independent, as in the single-site Hamiltonian of Section 2.2. In this case, if the RMS error of each individual summand is $\leq \mathcal{O}(\varepsilon)$ (for the Heisenberg-scaling ε of RPE), the RMS error of the linear combination is also $\leq \mathcal{O}(\varepsilon)$, since $\text{Var}(X + Y) = \text{Var}(X) + \text{Var}(Y)$ for independent random variables [67].

However, in the ancilla-free subroutines of Section 2.3, to learn the coefficients of a two-site Hamiltonian, the estimators being combined are not always independent. In particular, pairs of parameters are learned in parallel via the decoupling technique (ω_1 with ω_3 , ω_2 with ω_4 , and ξ_{12} with ξ_{34}). If decoupling were perfect, then the estimators obtained in parallel would be independent. In practice, since decoupling is approximate (as discussed in Appendix A), the estimators of parameters learned in parallel are not truly independent. Nevertheless, by the Cauchy-Schwarz inequality, the covariance of any two random variables X and Y , $\text{Cov}(X, Y)$, is bounded by $\text{Cov}(X, Y) \leq \sqrt{\text{Var}(X)\text{Var}(Y)}$ [67]. Additionally, $\text{Var}(X + Y) = \text{Var}(X) + \text{Var}(Y) + 2\text{Cov}(X, Y)$. Since each of the estimators being combined has RMS error $\leq \mathcal{O}(\varepsilon)$, these facts imply that their linear combinations also have RMS error $\leq \mathcal{O}(\varepsilon)$ as desired.

References

- [1] Arkopal Dutt, Edwin Pednault, Chai Wah Wu, Sarah Sheldon, John Smolin, Lev Bishop, and Isaac L. Chuang. Active learning of quantum system Hamiltonians yields query advantage. *Phys. Rev. Res.*, 5(3), July 2023. ISSN 2643-1564. doi: 10.1103/physrevresearch.5.033060. URL <http://dx.doi.org/10.1103/PhysRevResearch.5.033060>.
- [2] Tillmann Baumgratz and Animesh Datta. Quantum enhanced estimation of a multidimensional field. *Phys. Rev. Lett.*, 116(3):030801, January 2016. doi: 10.1103/PhysRevLett.116.030801. URL <http://dx.doi.org/10.1103/PhysRevLett.116.030801>.
- [3] Shengshi Pang and Todd A. Brun. Quantum metrology for a general Hamiltonian parameter. *Phys. Rev. A*, 90(2), August 2014. ISSN 1094-1622. doi: 10.1103/physreva.90.022117. URL <http://dx.doi.org/10.1103/PhysRevA.90.022117>.
- [4] Christopher Ferrie, Christopher E Granade, and David G Cory. How to best sample a periodic probability distribution, or on the accuracy of Hamiltonian finding strategies. *Quantum Inf. Process.*, 12:611–623, 2013. doi: 10.1007/s11128-012-0407-6. URL <http://dx.doi.org/10.1007/s11128-012-0407-6>.
- [5] Alexandr Sergeevich, Anushya Chandran, Joshua Combes, Stephen D. Bartlett, and Howard M. Wiseman. Characterization of a qubit Hamiltonian using adaptive measurements in a fixed basis. *Phys. Rev. A*, 84(5), November 2011. ISSN 1094-1622. doi: 10.1103/physreva.84.052315. URL <http://dx.doi.org/10.1103/PhysRevA.84.052315>.

- [6] Alejandra Valencia, Giuliano Scarcelli, and Yanhua Shih. Distant clock synchronization using entangled photon pairs. *Appl. Phys. Lett.*, 85(13):2655–2657, September 2004. ISSN 1077-3118. doi: 10.1063/1.1797561. URL <http://dx.doi.org/10.1063/1.1797561>.
- [7] D. Leibfried, M. D. Barrett, T. Schaetz, J. Britton, J. Chiaverini, W. M. Itano, J. D. Jost, C. Langer, and D. J. Wineland. Toward Heisenberg-limited spectroscopy with multiparticle entangled states. *Science*, 304(5676):1476–1478, 2004. doi: 10.1126/science.1097576. URL <https://www.science.org/doi/abs/10.1126/science.1097576>.
- [8] Mark de Burgh and Stephen D. Bartlett. Quantum methods for clock synchronization: Beating the standard quantum limit without entanglement. *Phys. Rev. A*, 72(4), October 2005. ISSN 1094-1622. doi: 10.1103/physreva.72.042301. URL <http://dx.doi.org/10.1103/PhysRevA.72.042301>.
- [9] Hwang Lee, Pieter Kok, and Jonathan P. Dowling. A quantum rosetta stone for interferometry. *J. Mod. Opt.*, 49(14–15):2325–2338, November 2002. ISSN 1362-3044. doi: 10.1080/0950034021000011536. URL <http://dx.doi.org/10.1080/0950034021000011536>.
- [10] Kirk McKenzie, Daniel A. Shaddock, David E. McClelland, Ben C. Buchler, and Ping Koy Lam. Experimental demonstration of a squeezing-enhanced power-recycled michelson interferometer for gravitational wave detection. *Phys. Rev. Lett.*, 88(23), May 2002. ISSN 1079-7114. doi: 10.1103/physrevlett.88.231102. URL <http://dx.doi.org/10.1103/PhysRevLett.88.231102>.
- [11] J. J. Bollinger, Wayne M. Itano, D. J. Wineland, and D. J. Heinzen. Optimal frequency measurements with maximally correlated states. *Phys. Rev. A*, 54:R4649–R4652, Dec 1996. doi: 10.1103/PhysRevA.54.R4649. URL <https://link.aps.org/doi/10.1103/PhysRevA.54.R4649>.
- [12] M. J. Holland and K. Burnett. Interferometric detection of optical phase shifts at the Heisenberg limit. *Phys. Rev. Lett.*, 71:1355–1358, Aug 1993. doi: 10.1103/PhysRevLett.71.1355. URL <https://link.aps.org/doi/10.1103/PhysRevLett.71.1355>.
- [13] D. J. Wineland, J. J. Bollinger, W. M. Itano, F. L. Moore, and D. J. Heinzen. Spin squeezing and reduced quantum noise in spectroscopy. *Phys. Rev. A*, 46:R6797–R6800, Dec 1992. doi: 10.1103/PhysRevA.46.R6797. URL <https://link.aps.org/doi/10.1103/PhysRevA.46.R6797>.
- [14] Carlton M. Caves. Quantum-mechanical noise in an interferometer. *Phys. Rev. D*, 23:1693–1708, Apr 1981. doi: 10.1103/PhysRevD.23.1693. URL <https://link.aps.org/doi/10.1103/PhysRevD.23.1693>.
- [15] Jianwei Wang, Stefano Paesani, Raffaele Santagati, Sebastian Knauer, Antonio A. Gentile, Nathan Wiebe, Maurangelo Petruzzella, Jeremy L. O’Brien, John G. Rarity, Anthony Laing, and Mark G. Thompson. Experimental quantum Hamiltonian learning. *Nat. Phys.*, 13(6):551–555, March 2017. ISSN 1745-2481. doi: 10.1038/nphys4074. URL <http://dx.doi.org/10.1038/nphys4074>.
- [16] Xiao-Liang Qi and Daniel Ranard. Determining a local Hamiltonian from a single eigenstate. *Quantum*, 3:159, July 2019. ISSN 2521-327X. doi: 10.22331/q-2019-07-08-159. URL <http://dx.doi.org/10.22331/q-2019-07-08-159>.
- [17] Nathan Wiebe, Christopher Granade, Christopher Ferrie, and David Cory. Quantum Hamiltonian learning using imperfect quantum resources. *Phys. Rev. A*, 89(4), April 2014. ISSN 1094-1622. doi: 10.1103/physreva.89.042314. URL <http://dx.doi.org/10.1103/PhysRevA.89.042314>.
- [18] Nathan Wiebe, Christopher Granade, Christopher Ferrie, and D. G. Cory. Hamiltonian learning and certification using quantum resources. *Phys. Rev. Lett.*, 112(19), May 2014. ISSN 1079-7114. doi: 10.1103/physrevlett.112.190501. URL <http://dx.doi.org/10.1103/PhysRevLett.112.190501>.

- [19] A. Shabani, M. Mohseni, S. Lloyd, R. L. Kosut, and H. Rabitz. Estimation of many-body quantum Hamiltonians via compressive sensing. *Phys. Rev. A*, 84:012107, Jul 2011. doi: 10.1103/PhysRevA.84.012107. URL <https://link.aps.org/doi/10.1103/PhysRevA.84.012107>.
- [20] Jun Zhang and Mohan Sarovar. Quantum Hamiltonian identification from measurement time traces. *Phys. Rev. Lett.*, 113(8), August 2014. ISSN 1079-7114. doi: 10.1103/physrevlett.113.080401. URL <http://dx.doi.org/10.1103/PhysRevLett.113.080401>.
- [21] Tim J. Evans, Robin Harper, and Steven T. Flammia. Scalable bayesian Hamiltonian learning, 2019. URL <https://arxiv.org/abs/1912.07636>.
- [22] Zhi Li, Liujun Zou, and Timothy H. Hsieh. Hamiltonian tomography via quantum quench. *Phys. Rev. Lett.*, 124(16), April 2020. ISSN 1079-7114. doi: 10.1103/physrevlett.124.160502. URL <http://dx.doi.org/10.1103/PhysRevLett.124.160502>.
- [23] Assaf Zubida, Elad Yitzhaki, Netanel H. Lindner, and Eyal Bairey. Optimal short-time measurements for Hamiltonian learning, 2021. URL <http://arxiv.org/abs/2108.08824>.
- [24] Davide Rattacaso, Gianluca Passarelli, and Procolo Lucignano. High-accuracy Hamiltonian learning via delocalized quantum state evolutions. *Quantum*, 7:905, January 2023. ISSN 2521-327X. doi: 10.22331/q-2023-01-26-905. URL <http://dx.doi.org/10.22331/q-2023-01-26-905>.
- [25] Wenjun Yu, Jinzhao Sun, Zeyao Han, and Xiao Yuan. Robust and efficient Hamiltonian learning. *Quantum*, 7:1045, June 2023. ISSN 2521-327X. doi: 10.22331/q-2023-06-29-1045. URL <http://dx.doi.org/10.22331/q-2023-06-29-1045>.
- [26] Daniel Burgarth, Koji Maruyama, and Franco Nori. Indirect quantum tomography of quadratic Hamiltonians. *New J. Phys.*, 13(1):013019, January 2011. ISSN 1367-2630. doi: 10.1088/1367-2630/13/1/013019. URL <http://dx.doi.org/10.1088/1367-2630/13/1/013019>.
- [27] Daniel Stilck França, Liubov A. Markovich, V. V. Dobrovitski, Albert H. Werner, and Johannes Borregaard. Efficient and robust estimation of many-qubit Hamiltonians, 2022. URL <http://arxiv.org/abs/2205.09567>.
- [28] Anurag Anshu, Srinivasan Arunachalam, Tomotaka Kuwahara, and Mehdi Soleimanifar. Sample-efficient learning of interacting quantum systems. *Nat. Phys.*, 17(8):931–935, May 2021. ISSN 1745-2481. doi: 10.1038/s41567-021-01232-0. URL <http://dx.doi.org/10.1038/s41567-021-01232-0>.
- [29] Jeongwan Haah, Robin Kothari, and Ewin Tang. Optimal learning of quantum Hamiltonians from high-temperature Gibbs states, 2023. URL <http://arxiv.org/abs/2108.04842>.
- [30] Faris M. Sbahi, Antonio J. Martinez, Sahil Patel, Dmitri Saberi, Jae Hyeon Yoo, Geoffrey Roeder, and Guillaume Verdon. Provably efficient variational generative modeling of quantum many-body systems via quantum-probabilistic information geometry, 2022. URL <http://arxiv.org/abs/2206.04663>.
- [31] Guillaume Verdon, Jacob Marks, Sasha Nanda, Stefan Leichenauer, and Jack Hidary. Quantum Hamiltonian-based models and the variational quantum thermalizer algorithm, 2019. URL <http://arxiv.org/abs/1910.02071>.
- [32] H. Y. Kwon, H. G. Yoon, C. Lee, G. Chen, K. Liu, A. K. Schmid, Y. Z. Wu, J. W. Choi, and C. Won. Magnetic Hamiltonian parameter estimation using deep learning techniques. *Science Advances*, 6(39): eabb0872, 2020. doi: 10.1126/sciadv.abb0872. URL <https://www.science.org/doi/abs/10.1126/sciadv.abb0872>.
- [33] Dingchen Wang, Songrui Wei, Anran Yuan, Fanghua Tian, Kaiyan Cao, Qizhong Zhao, Dezhen Xue, and Sen Yang. Machine learning magnetic parameters from spin configurations, 2019. URL <http://arxiv.org/abs/1908.05829>.

- [34] Hsin-Yuan Huang, Richard Kueng, and John Preskill. Predicting many properties of a quantum system from very few measurements. *Nat. Phys.*, 16(10):1050–1057, June 2020. ISSN 1745-2481. doi: 10.1038/s41567-020-0932-7. URL <http://dx.doi.org/10.1038/s41567-020-0932-7>.
- [35] Hsin-Yuan Huang, Yu Tong, Di Fang, and Yuan Su. Learning many-body Hamiltonians with Heisenberg-limited scaling. *Phys. Rev. Lett.*, 130(20), May 2023. ISSN 1079-7114. doi: 10.1103/physrevlett.130.200403. URL <http://dx.doi.org/10.1103/PhysRevLett.130.200403>.
- [36] Haoya Li, Yu Tong, Hongkang Ni, Tuvia Gefen, and Lexing Ying. Heisenberg-limited Hamiltonian learning for interacting bosons, 2023. URL <http://arxiv.org/abs/2307.04690>.
- [37] Alicja Dutkiewicz, Thomas E. O’Brien, and Thomas Schuster. The advantage of quantum control in many-body Hamiltonian learning, 2023. URL <http://arxiv.org/abs/2304.07172>.
- [38] Michael A. Nielsen. *Quantum computation and quantum information*. Cambridge University Press, Cambridge ; New York, 2000. ISBN 0521632358.
- [39] Agnes Valenti, Evert van Nieuwenburg, Sebastian Huber, and Eliska Greplova. Hamiltonian learning for quantum error correction. *Phys. Rev. Res.*, 1(3), November 2019. ISSN 2643-1564. doi: 10.1103/physrevresearch.1.033092. URL <http://dx.doi.org/10.1103/PhysRevResearch.1.033092>.
- [40] Nathan Wiebe, Christopher Granade, and D G Cory. Quantum bootstrapping via compressed quantum Hamiltonian learning. *New J. Phys.*, 17(2):022005, February 2015. ISSN 1367-2630. doi: 10.1088/1367-2630/17/2/022005. URL <http://dx.doi.org/10.1088/1367-2630/17/2/022005>.
- [41] Dominik Hangleiter, Ingo Roth, Jonas Fuksa, Jens Eisert, and Pedram Roushan. Robustly learning the Hamiltonian dynamics of a superconducting quantum processor, 2024. URL <http://arxiv.org/abs/2108.08319>.
- [42] Marcus P. da Silva, Olivier Landon-Cardinal, and David Poulin. Practical characterization of quantum devices without tomography. *Phys. Rev. Lett.*, 107(21), November 2011. ISSN 1079-7114. doi: 10.1103/physrevlett.107.210404. URL <http://dx.doi.org/10.1103/PhysRevLett.107.210404>.
- [43] Shelby Kimmel, Guang Hao Low, and Theodore J. Yoder. Robust calibration of a universal single-qubit gate set via robust phase estimation. *Phys. Rev. A*, 92(6), December 2015. ISSN 1094-1622. doi: 10.1103/physreva.92.062315. URL <http://dx.doi.org/10.1103/PhysRevA.92.062315>.
- [44] Antonio E. Russo, William M. Kirby, Kenneth M. Rudinger, Andrew D. Baczewski, and Shelby Kimmel. Consistency testing for robust phase estimation. *Phys. Rev. A*, 103(4), April 2021. ISSN 2469-9934. doi: 10.1103/physreva.103.042609. URL <http://dx.doi.org/10.1103/PhysRevA.103.042609>.
- [45] Federico Belliardo and Vittorio Giovannetti. Achieving Heisenberg scaling with maximally entangled states: An analytic upper bound for the attainable root-mean-square error. *Phys. Rev. A*, 102(4), October 2020. ISSN 2469-9934. doi: 10.1103/physreva.102.042613. URL <http://dx.doi.org/10.1103/PhysRevA.102.042613>.
- [46] Hongkang Ni, Haoya Li, and Lexing Ying. Quantum Hamiltonian learning for the Fermi-Hubbard model, 2023. URL <http://arxiv.org/abs/2312.17390>.
- [47] Frederik Görg, Kilian Sandholzer, Joaquín Minguzzi, Rémi Desbuquois, Michael Messer, and Tilman Esslinger. Realization of density-dependent peierls phases to engineer quantized gauge fields coupled to ultracold matter. *Nat. Phys.*, 15(11):1161–1167, August 2019. ISSN 1745-2481. doi: 10.1038/s41567-019-0615-4. URL <http://dx.doi.org/10.1038/s41567-019-0615-4>.
- [48] K. Çeven, M. Ö. Oktel, and A. Keleş. Neural-network quantum states for a two-leg Bose-Hubbard ladder under magnetic flux. *Phys. Rev. A*, 106(6), December 2022. ISSN 2469-9934. doi: 10.1103/physreva.106.063320. URL <http://dx.doi.org/10.1103/PhysRevA.106.063320>.

- [49] Gerald D Mahan. *Many-particle physics*. Physics of solids and liquids. Kluwer Academic/Plenum Publishers, New York, 3rd ed. edition, 2000. ISBN 0306463385.
- [50] M Ulmke, V Janiš, and Dieter Vollhardt. Anderson-Hubbard model in infinite dimensions. *Phys. Rev. B*, 51(16):10411, 1995. URL <https://doi.org/10.1103/PhysRevB.51.10411>.
- [51] Nathan Giovanni, Marcello Civelli, and Maria CO Aguiar. Anderson localization effects on the doped Hubbard model. *Phys. Rev. B*, 103(24):245134, 2021. URL <https://doi.org/10.1103/PhysRevB.103.245134>.
- [52] Lawrence W. Cheuk, Matthew A. Nichols, Melih Okan, Thomas Gersdorf, Vinay V. Ramasesh, Waseem S. Bakr, Thomas Lompe, and Martin W. Zwierlein. Quantum-gas microscope for fermionic atoms. *Phys. Rev. Lett.*, 114(19), May 2015. ISSN 1079-7114. doi: 10.1103/physrevlett.114.193001. URL <http://dx.doi.org/10.1103/PhysRevLett.114.193001>.
- [53] Elmar Haller, James Hudson, Andrew Kelly, Dylan A. Cotta, Bruno Peaudecerf, Graham D. Bruce, and Stefan Kuhr. Single-atom imaging of fermions in a quantum-gas microscope. *Nat. Phys.*, 11(9):738–742, July 2015. ISSN 1745-2481. doi: 10.1038/nphys3403. URL <http://dx.doi.org/10.1038/nphys3403>.
- [54] Peter T. Brown, Debayan Mitra, Elmer Guardado-Sanchez, Peter Schauß, Stanimir S. Kondov, Ehsan Khatami, Thereza Paiva, Nandini Trivedi, David A. Huse, and Waseem S. Bakr. Spin-imbalance in a 2d Fermi-Hubbard system. *Science*, 357(6358):1385–1388, September 2017. ISSN 1095-9203. doi: 10.1126/science.aam7838. URL <http://dx.doi.org/10.1126/science.aam7838>.
- [55] Thomas Hartke, Botond Oreg, Ningyuan Jia, and Martin Zwierlein. Doublon-hole correlations and fluctuation thermometry in a Fermi-Hubbard gas. *Phys. Rev. Lett.*, 125(11), September 2020. ISSN 1079-7114. doi: 10.1103/physrevlett.125.113601. URL <http://dx.doi.org/10.1103/PhysRevLett.125.113601>.
- [56] Joannis Koepsell, Sarah Hirthe, Dominik Bourgund, Pimonpan Sompert, Jayadev Vijayan, Guillaume Salomon, Christian Gross, and Immanuel Bloch. Robust bilayer charge pumping for spin- and density-resolved quantum gas microscopy. *Phys. Rev. Lett.*, 125(1), July 2020. ISSN 1079-7114. doi: 10.1103/physrevlett.125.010403. URL <http://dx.doi.org/10.1103/PhysRevLett.125.010403>.
- [57] Anant Kale, Jakob Hendrik Huhn, Muqing Xu, Lev Haldar Kendrick, Martin Lebrat, Christie Chiu, Geoffrey Ji, Fabian Grusdt, Annabelle Bohrdt, and Markus Greiner. Schrieffer-wolff transformations for experiments: Dynamically suppressing virtual doublon-hole excitations in a Fermi-Hubbard simulator. *Phys. Rev. A*, 106(1), July 2022. ISSN 2469-9934. doi: 10.1103/physreva.106.012428. URL <http://dx.doi.org/10.1103/PhysRevA.106.012428>.
- [58] Muqing Xu, Lev Haldar Kendrick, Anant Kale, Youqi Gang, Geoffrey Ji, Richard T. Scalettar, Martin Lebrat, and Markus Greiner. Frustration- and doping-induced magnetism in a Fermi-Hubbard simulator. *Nature*, 620(7976):971–976, August 2023. ISSN 1476-4687. doi: 10.1038/s41586-023-06280-5. URL <http://dx.doi.org/10.1038/s41586-023-06280-5>.
- [59] Martin Lebrat, Muqing Xu, Lev Haldar Kendrick, Anant Kale, Youqi Gang, Pranav Seetharaman, Ivan Morera, Ehsan Khatami, Eugene Demler, and Markus Greiner. Observation of nagaoka polarons in a Fermi-Hubbard quantum simulator, 2023. URL <https://arxiv.org/abs/2308.12269>.
- [60] Patrik Fazekas. *Lecture Notes on Electron Correlation and Magnetism*, volume 5. World Scientific, 1999.
- [61] Hongkang Ni, Haoya Li, and Lexing Ying. On low-depth algorithms for quantum phase estimation. *Quantum*, 7:1165, November 2023. ISSN 2521-327X. doi: 10.22331/q-2023-11-06-1165. URL <http://dx.doi.org/10.22331/q-2023-11-06-1165>.

- [62] Sergey Bravyi. Lagrangian representation for fermionic linear optics, 2004. URL <http://arxiv.org/abs/quant-ph/0404180>.
- [63] Nicetu Tibau Vidal, Mohit Lal Bera, Arnau Riera, Maciej Lewenstein, and Manabendra Nath Bera. Quantum operations in an information theory for fermions. *Phys. Rev. A*, 104(3), September 2021. ISSN 2469-9934. doi: 10.1103/physreva.104.032411. URL <http://dx.doi.org/10.1103/PhysRevA.104.032411>.
- [64] Earl Campbell. Random compiler for fast Hamiltonian simulation. *Phys. Rev. Lett.*, 123(7), August 2019. ISSN 1079-7114. doi: 10.1103/physrevlett.123.070503. URL <http://dx.doi.org/10.1103/PhysRevLett.123.070503>.
- [65] Marin Bukov and Lode Pollet. Mean-field phase diagram of the Bose-Fermi Hubbard model. *Phys. Rev. B*, 89(9), March 2014. ISSN 1550-235X. doi: 10.1103/physrevb.89.094502. URL <http://dx.doi.org/10.1103/PhysRevB.89.094502>.
- [66] E.T. Jaynes and F.W. Cummings. Comparison of quantum and semiclassical radiation theories with application to the beam maser. *Proc. IEEE*, 51(1):89–109, 1963. ISSN 0018-9219.
- [67] Geoffrey Grimmett and David Stirzaker. *Probability and random processes*. Oxford University Press, Oxford; New York, 3rd ed. edition, 2001. ISBN 0198572239.